International Journal of Nanomedicine

Dovepress
open access to scientific and medical research

Open Access Full Text Article

ORIGINAL RESEARCH

Role of Au(NPs) in the enhanced response of Au(NPs)-decorated MWCNT electrochemical biosensor

This article was published in the following Dove Press journal:
International Journal of Nanomedicine

Shahid Mehmood[1]
Regina Ciancio[2]
Elvio Carlino[2,3]
Arshad S Bhatti[1]

[1]Department of Physics, Center for Micro and Nano Devices, COMSATS Institute of Information Technology, Islamabad, Pakistan; [2]CNR-IOM TASC, Trieste, Italy; [3]CNR-IMM, Campus Universitario, Via per Monteroni, Lecce, Italy

Background: The combination of Au-metallic-NPs and CNTs are a new class of hybrid nanomaterials for the development of electrochemical biosensor. Concentration of Au(nanoparticles [NPs]) in the electrochemical biosensor is crucial for the efficient charge transfer between the Au-NPs-MWCNTs modified electrode and electrolytic solution.

Methods: In this work, the charge transfer kinetics in the glassy carbon electrode (GCE) modified with Au(NPs)–multiwalled carbon nanotube (MWCNT) nanohybrid with varied concentrations of Au(NPs) in the range 40–100 nM was studied using electrochemical impedance spectroscopy (EIS). Field emission scanning electron microscopy and transmission electron microscopy confirmed the attachment of Au(NPs) on the surface of MWCNTs.

Results: The cyclic voltammetry and EIS results showed that the charge transfer mechanism was diffusion controlled and the rate of charge transfer was dependent on the concentration of Au(NPs) in the nanohybrid. The formation of spherical diffusion zone, which was dependent on the concentration of Au(NPs) in nanohybrids, was attributed to result in 3 times the increase in the charge transfer rate k_s, 5 times increase in mass transfer, and 5% (9%) increase in I_{pa} (I_{pc}) observed in cyclic voltammetry in 80 nM Au(NP) nanohybrid-modified GCE from MWCNT-modified GCE. The work was extended to probe the effect of charge transfer rates at various concentrations of Au(NPs) in the nanohybrid-modified electrodes in the presence of Escherichia coli. The cyclic voltammetry results clearly showed the best results for 80 nM Au(NPs) in nanohybrid electrode.

Conclusion: The present study suggested that the formation of spherical diffusion zone in nanohybrid-modified electrodes is critical for the enhanced electrochemical biosensing applications.

Keywords: multiwalled carbon nanotubes, Au nanoparticle–MWCNT nanohybrids, cyclic voltammetery, electrochemical impedance spectroscopy

Introduction

In recent years, nanomaterials because of specific electrical, optical, magnetic, chemical, and mechanical properties have garnered attention in many upstream fields.[1–4] These fields include diagnostics, drug delivery, artificial photosynthesis,[5] molecular recognition in therapeutics,[6] electrochemical biologic or chemical sensor,[7] solar energy harvesting,[8] photosynthesis, and biochemical sensing.[9] Out of different classes of nanomaterials, the use of metallic nanoparticles (NPs) in electrochemical sensors has received much attention because of their unique role in transfer of free charge to enhance conductivity, and catalytic and photocatalytic activity.[10–13] Metallic NPs, for example, Au or Ag, for the detection of biologic molecules have been the center of attraction because of their exceptional biocompatibility. On the other hand, carbon nanotubes (CNTs) since their discovery in 1991[14] have gained immense interest as a potential candidate in a wide

Correspondence: Shahid Mehmood
Department of Physics, Center for Micro and Nano Devices, COMSATS Institute of Information Technology, Park Road Campus, Islamabad 44500, Pakistan
Tel +92 51 901 9191
Email shahidm@comsats.edu.pk

submit your manuscript | www.dovepress.com
Dovepress
http://dx.doi.org/10.2147/IJN.S155388

range of applications in electrochemistry.[15] The combination of metallic NPs and CNTs has created a new class of hybrid nanomaterials with multifunctional properties[16–19] for potential use in optical, catalytic, sensor, solar cells, and most importantly in biosensor applications.[20–23] The ability of Au(NPs) to adsorb proteins combined with the catalytic properties of CNTs has encouraged the use of Au(NP)–CNT nanohybrids for the development of electrochemical enzyme-based biosensors.[24] It has been demonstrated that several enzymes were able to preserve their enzymatic and electrochemical activity even after they were immobilized on the colloidal Au(NPs).[25]

The decoration of metallic NPs on multiwalled carbon nanotubes (MWCNTs) has been shown to enhance the conductivity of electrochemical sensors. Hrapovic et al[26] used both nafion-coated single-walled carbon nanotubes (SWCNTs) and Pt(NPs) for the detection of low concentration of hydrogen peroxide (H_2O_2), which was better compared to SWCNTs or Pt(NPs) alone. Au-functionalized MWCNTs have also been employed as a sensing platform in electrochemical sensing of hydroxylamine, paraoxon, laccase from trametes versicolor extracts, and glycan assay on living cancer cells.[27–30] Li et al[31] reported the facilitated mass transport in acetylene electro-oxidation reaction in Au–MWCNTs, which resulted in low onset potential and high current density compared to either Au(NPs) or Au catalysts. Several works on composites such as Au(NP)/poly(amidoamine)–MWCNT–Chi nanocomposite-modified glassy carbon electrode (GCE),[32] Au(NPs)/MWCNT–CS composites,[33] CD/Au(NP)/MWCNT composites and MWCNT,[34] and Au(NPs)/MWCNTS/reduced graphene oxide[35] have shown their use as sensors with great sensitivity and reproducibility.

The development of techniques for efficient and sensitive bacterial detection is the goal of current research in nanomaterial-based electrochemical immunosensors. Microbes in direct contact with the GCE have less efficiency of electron transfer from the bacterial cell to anode in the absence of a mediator. The cytoplasmic membrane in microbes acts as a barrier that blocks electron transfer from the microbes to the neighboring environments. A few strategies have been demonstrated for direct or indirect electron transfer to the working electrode, which include membrane proteins or cell metabolites or through electrically conductive nanowires.[36,37] Park and Zeikus suggested the efficient charge transfer from microbes to anode in the presence of mediators such as thionine, methylene blue, and 2-hydroxyl 1, 4-naphthoquinone.[38] The use of the above-mentioned mediators overcomes the cytoplasmic membrane barrier and facilitates the electron transfer. *Escherichia coli*, one of the readily available and easily grown bacterial strains, can transfer electrons from electrochemical active microorganisms to electrode through mediators.[39,40] CNTs because of excellent electronic conductivity, easy functionalization, and remarkable chemical stability have been recognized as an ideal electroactive material for their use as a mediator. Recently, dendrimers,[41] Au(NPs),[42] and quantum dot[43]-based immunosensors have been developed for the detection of antibodies, peptides, and DNA. The use of Au(NP) and CNT composites has attracted considerable attention because of enhanced loading capability of Au(NPs) with active biomolecules that improves the recognition ratio and binding affinity. The Au(NP)–CNT composite is advantageous because of the biocompatibility of CNTs. The role of the concentration of Au(NPs) is crucial in the sensing efficiency of Au(NP)–MWCNT-modified electrodes used in electrochemical immunosensors. It is important to note that any variation in the concentration of Au(NPs) in the modified electrodes of electrochemical immunosensors affects the rate of charge transfer between the modified electrode and electrolytic solution. The objective of the present study was to explore the kinetics of charge transfer in the Au(NP)–MWCNT-modified GCE in a biologic reaction.

In this paper, different concentrations of Au(NPs) ranging from 40 to 100 nM were functionalized on the surface of acid-treated MWCNTs to form Au(NP)–MWCNT nanohybrids. The GCE was then modified with nanohybrids to measure the electrochemical response. The nature of the reaction processes, rate of charge transfer, and number of electrons transferred were determined by the cyclic voltammetry (CV), which was performed at different scan rates (from 50 to 300 mV s^{-1}) in 0.1 mol L^{-1} potassium ferricyanide ($K_4[Fe(CN)_6]$). The electrochemical impedance spectroscopy (EIS) was employed to determine the charge transfer characteristics for different concentrations of Au(NPs) in nanohybrid-modified GCE. Finally, CV scans at the rate of 50 mV s^{-1} were performed on nanohybrid-modified electrodes in various concentrations of *E. coli* (from 10^4 to 10^6/mL) to determine the efficiency of the modified electrode.

Experiments

Synthesis of Au(NPs)

By using gold(III) chloride hydrate (Sigma-Aldrich Co., St Louis, MO, USA), 1 mM gold salt solution was prepared and refluxed in a round bottom flask with a continuous stirring for 10 minutes. In 100 mL of deionized (DI) water, 40 mM sodium citrate solution (Sigma-Aldrich) was added separately and the mixture was heated at 65°C±5°C for 30 minutes. The hot solution was then mixed with the Au salt solution followed by reflux for another 45 minutes. The solution was then cooled to room temperature and filtered using Whatman

filter paper leading to the formation of citrate-stabilized Au(NPs). The synthesized NPs appeared bright red in color.

Formation of Au(NP)–MWCNT nanohybrids

Pristine MWCNTs (purchased from Beijing DK Nontechnology, Beijing, China) were first oxidized by adding in 40 mL acidic mixture of H_2SO_4/HNO_3 with 3:1 ratio and ultrasonicated for 6 hours. The oxidized MWCNTs were then vacuum filtered, washed by DI water several times to remove the acidic contents, and dried overnight in an oven at 60°C. The dried oxidized MWCNTs were then dispersed in 2 mL of DI water to form four suspension solutions. The synthesized Au(NPs) with concentrations of 40, 60, 80, and 100 nM were added in 2 mL DI water and then mixed in all four oxidize MWCNT suspension solutions. The mixture was then ultrasonicated for 2 hours to form the nanohybrids of Au(NPs) with MWCNTs and afterwards annealed at 150°C to strengthen the attachment of Au(NPs) on the surface of MWCNTs.

Modification of GCE with MWCNTs and Au(NP)–MWCNT nanohybrids

The GCE was first cleaned by 0.3 μm alumina powder followed by ultrasonic bath in ethanol for 10 minutes. Five milligrams of oxidized MWCNTs was added in 5 mL of DI water and then ultrasonicated for 60 minutes to form the homogeneous solution. Ten microliters of the prepared solution was then dropped on the surface of cleaned GCE. The GCE was then dried under the lamp for 30 minutes and rinsed in DI water several times. The same procedure was repeated to modify the GCE with different concentrations of Au(NP)–MWCNT nanohybrids. The electrodes modified with each concentration were also incubated for 30 minutes in different concentrations of *E. coli* in the range from 10^4 to 10^6/mL.

Electrochemical studies were carried out using Metrohm 85695 Autolab – Electrochemical Analyzer with Nova 1.10 software. Platinum sheet was used as a counter electrode while Ag/AgCl electrode was used as a reference electrode. CV was performed at various scan rates in the range from 0.05 to 0.35 V s^{-1} with an increment of 0.05 V s^{-1}. The pH during the experiment was 7, while all the experiments were performed at room temperature. EIS was carried out in the frequency range of 100 kHz to 100 mHz.

Results and discussion

Confirmation of the attachment of the Au(NPs) on the surface of MWCNTs was done by using field emission scanning electron microscopy (FESEM) and transmission electron microscopy (TEM). Figure 1A and B shows the FESEM images of MWCNTs (Figure 1A) and Au(NP)–MWCNT nanohybrids (Figure 1B). The appearance of white spot in Figure 1B in comparison to Figure 1A was due to attachment of Au(NPs) on the surface of MWCNTs. From Figure 1B, it can also be seen that the Au(NPs) were agglomerated on the surface of MWCNTs. For further confirmation of attachment of Au(NPs), TEM was performed, and Figure 1C and D shows the TEM images of MWNTs and Au(NP)–MWCNT nanohybrids, respectively. Au(NPs) appeared as randomly dispersed sphere on the surface of the MWCNTs as shown in Figure 1D. The average diameter of the MWCNTs determined from the TEM micrographs was 40±5 nm, while that of Au(NPs) was 20±5 nm. FESEM and TEM images confirmed the random immobilization of Au(NPs) on the surface of the MWCNTs and large agglomerated particles were also observed.

X-ray photoelectron spectroscopy (XPS) performed on similar hybrids has shown that three peaks at 283.7±0.2, 284.8±0.2, and 290.4±0.2 eV are due to the sp^2 hybridized graphic carbon atoms, sp^3 hybridization, and π-plasmon excitations, respectively, of C-1s atom in MWCNTs.[44] Decoration of metal catalysts such as Au has introduced new peak in XPS because of Au-4f7/2 at 83.7±0.2 eV.[45] We have recently demonstrated the formation of Au(NP)–MWCNT nanohybrids,[46] which confirmed that both acid treatment and functionalization of Au(NPs) introduced stresses on the surface of MWCNTs as studied by the X-ray diffraction and Raman spectroscopy (Figures 6–8).[46] Linear decrease in D/G ratio in Raman spectra from 1.27 for oxidized MWCNTs to 1.03 for 80 nM Au(NPs) concentrations and then again an increase to 1.21 for 100 nM Au(NPs) on the surface of MWCNTs was the significant signature of Au(NPs) functionalization.

Effect of scan rate

The CV profiles of the bare, MWCNT-, and Au(NP)–MWCNT-modified GCEs in 0.1 mol L^{-1} $K_4[Fe(CN)_6]$ taken at various scan rates from 0.05 to 0.3 V s^{-1} are shown in Figure 2A–F. Where Figure 2A represents bare, Figure 2B represents MWCNT-modified, and Figure 2C–F 40–100 nM Au(NP)–MWCNT-modified GCEs. The hysteresis loops showed well-defined redox peaks due to oxidation or reduction of $[Fe(CN)^6]^{4-}$ ions. The positive current in Figure 2 was due to the oxidation current I_{pc} and the peak in current was observed at the corresponding cathodic potential, while negative current represented the reduction current I_{pa} and an inverted peak in the reduction current was observed at the corresponding anodic potential E_{pa}. It was observed that the I_{pc} and I_{pa} increased gradually and E_{pc} and E_{pa} shifted to high and low voltages, respectively, with the increase in

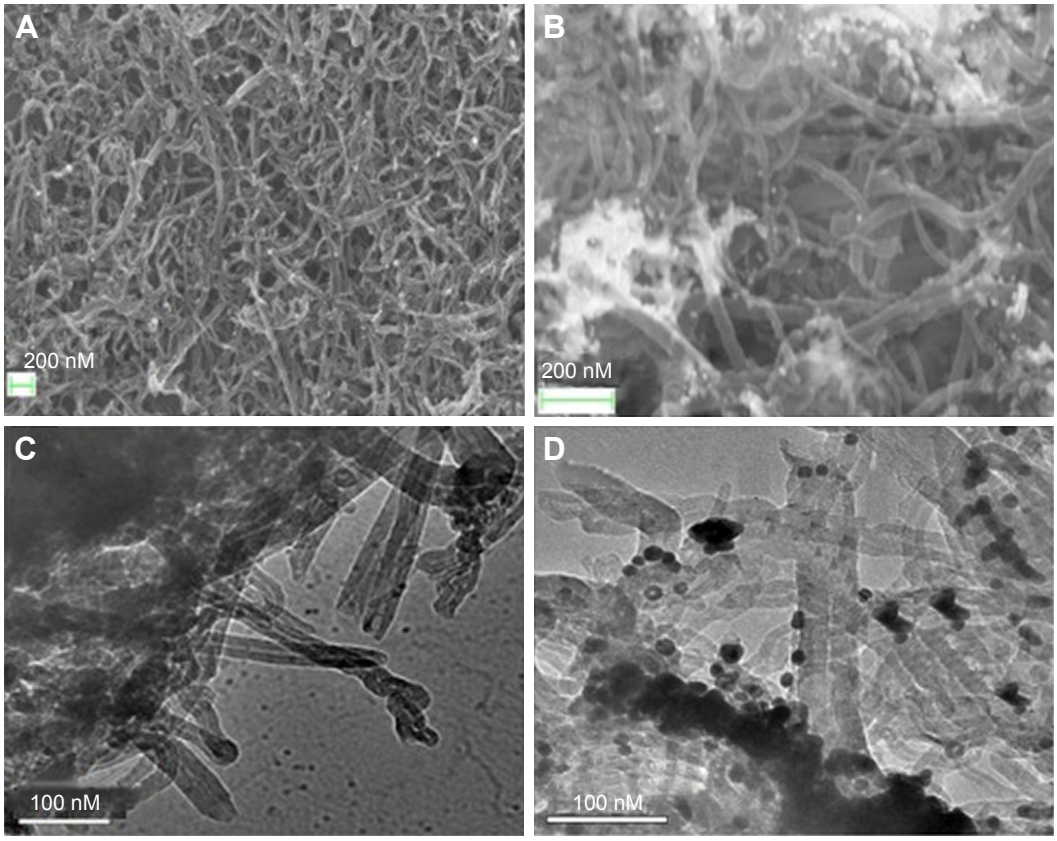

Figure 1 FESEM images of (**A**) MWCNTs, (**B**) Au(NP)–MWCNT nanohybrids. TEM images of (**C**) MWCNTs and (**D**) Au(NP)–MWCNT nanohybrids.
Note: FESEM and TEM confirmed the immobilization of Au(NPs) on the surface of MWCNTs.
Abbreviations: Au(NPs), Au nanoparticles; FESEM, field emission scanning electron microscopy; MWCNTs, multiwalled carbon nanotubes; TEM, transmission electron microscopy.

scan rates. Emergence of new reduction peak at 0.8 V with increased concentration of Au(NPs) was due to $[Fe(CN)_6]^{3-}$ ions reduction.[32]

A linear correlation was observed between the log (I) and log (*v*) with a correlation coefficient® >95% for the bare and modified electrodes as shown in Figure 3. The slope of log (I_{pa}) vs log (*v*) was in the range from –0.41±0.01 to –0.48±0.01, while for log (I_{pc}) and log (*v*), the slope was in the range from 0.51±0.02 to 0.67±0.04 for the bare, MWCNT-, and Au(NP)–MWCNT-modified GCEs. The determined slopes were close to the theoretically value of 0.50 for a purely diffusion-controlled current,[47] which confirmed that the redox processes at the surface of modified electrode were diffusion controlled. The small values of slope for I_{pa} represented the slow diffusion of heavier $[Fe(CN)^6]^{4-}$ ions with respect to the diffusion of K^+ ions. It was important to know if the diffusion-controlled processes involved in the redox reaction were reversible, quasi-reversible, or irreversible, which could give an insight about the charge transfer rate. In a reversible reaction, cathodic peak potential E_{pa} is usually independent of the scan rate "*v*". However, in the present case, from Figure 2, E_{pa} showed dependence on the scan rate for all modified GCEs as given in Laviron's model Equation 1.[48] Laviron's equation is used for many sensor applications, which claim that the use of modified electrodes produced peaks in CV curves. Laviron's equation is successfully applied to modified electrode system for determining the electron transfer rate constant where reaction kinetics dominates the system.[49–51]

$$E_p = E_{1/2} + \frac{RT}{\alpha n_\alpha F}\left[0.780 + \ln\left(\frac{D_R^{1/2}}{k_s}\right) + \ln\left(\frac{\alpha n_\alpha F v}{RT}\right)^{1/2}\right] - \frac{RT}{\alpha n_\alpha F}\ln v^{1/2} \quad (1)$$

where n_α is the number of electrons, k_s the charge transfer rate constant, D_R ($cm^2\ s^{-1}$) the diffusion coefficient, C_R (mol cm^{-3}) the concentration of $K_4[Fe(CN)_6]$, T (K) is absolute temperature, R (J $mol^{-1}\ K^{-1}$) the gas constant, α the energy transfer coefficient, $E_{1/2}$ the half-wave potential, and F (C/mol) is the Faraday constant.

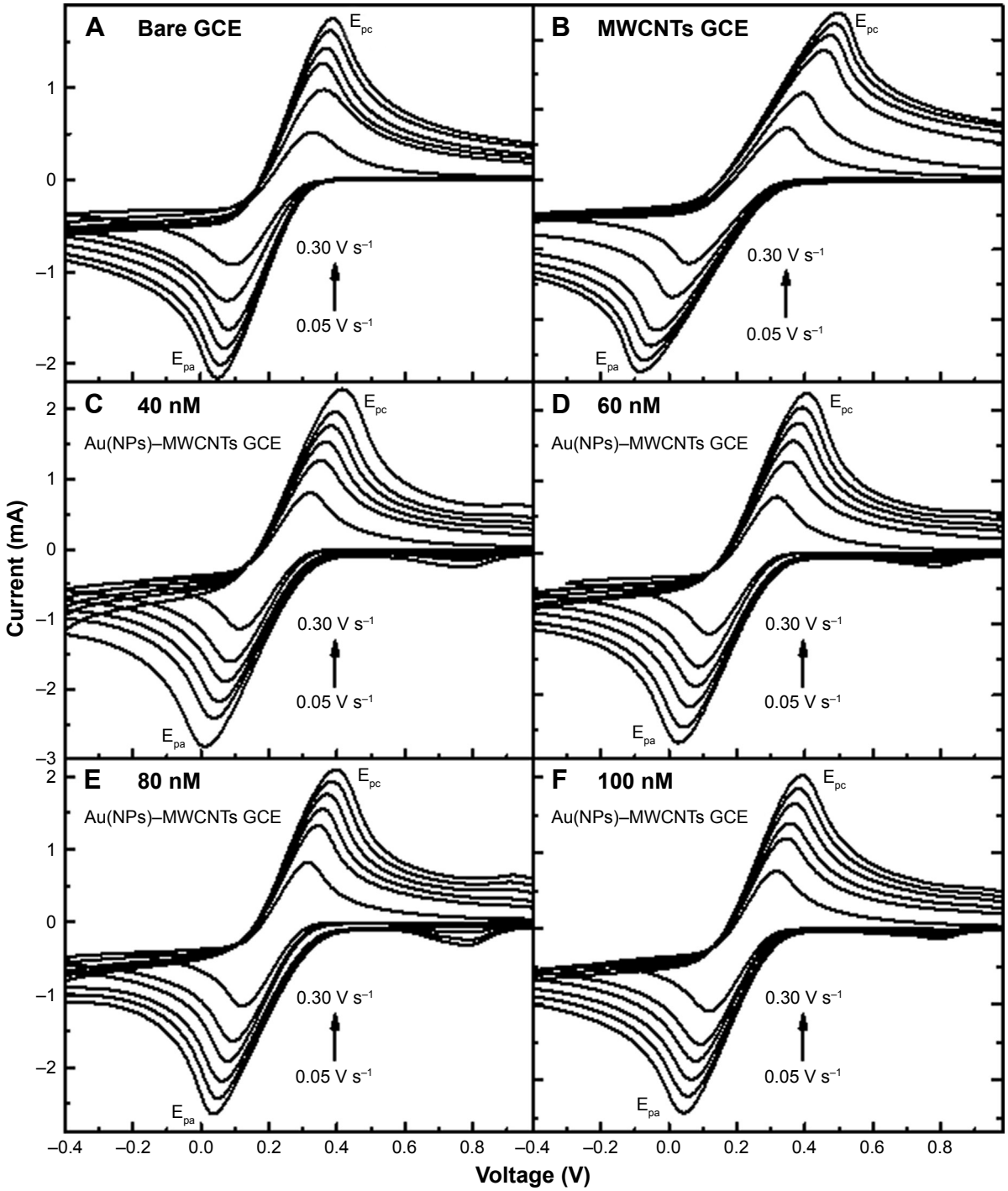

Figure 2 CV scans of GCE, MWCNTs-modified GCE, and Au(NP)–MWCNT-modified GCE in 0.1 mol L^{-1} $K_4[Fe(CN)_6]$ with scan rates 0.05, 0.1, 0.15, 0.2, 0.25, and 0.3 V s^{-1}.
Note: (**A**) GCE, (**B**) MWCNT-modified GCE, (**C**) 40 nM Au(NP)–MWCNT-modified GCE, (**D**) 60 nM Au(NP)–MWCNT-modified GCE, (**E**) 80 nM Au(NP)–MWCNT-modified GCE, and (**F**) 100 nM Au(NP)–MWCNT-modified GCE.
Abbreviations: Au(NPs), Au nanoparticles; CV, cyclic voltammetery; GCE, glassy carbon electrode; MWCNTs, multiwalled carbon nanotubes.

According to Equation 1, E_{pa} linearly depends on ln $v^{1/2}$ as shown in Figure 4A for bare, MWCNT-, and Au(NP)–MWCNT-modified GCEs (only bare GCE and 100 Au(NP)–MWCNT-modified GCEs are shown), and its slope is inversely proportional to the product (αn_α) expressed in Equation 2 and used to determine the product αn_α.

$$-\frac{RT}{\alpha n_\alpha F} = \text{slope}\,(E_{pa}\, vs\, ln v^{1/2}) \quad (2)$$

The cathodic peak potential, E_{pc}, also depended linearly on the scan rate as shown in Figure 4B. The *y*-intercept at

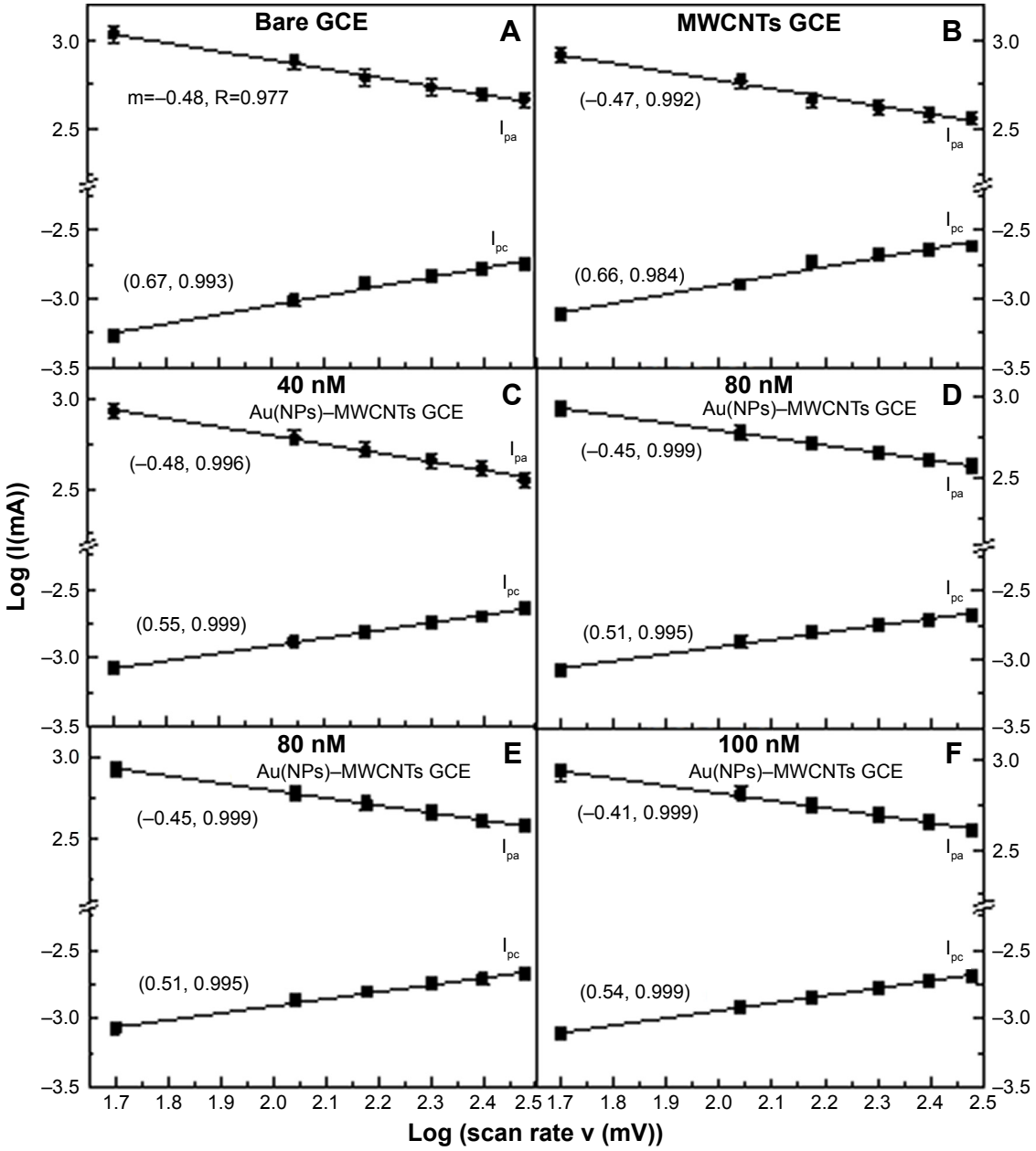

Figure 3 Plots of log (I_{pc}) and log (I_{pa}) as a function of log of scan rates in mV s^{-1}.
Notes: (**A**) GCE, (**B**) MWCNT-modified GCE, and (**C**–**F**) 40–100 nM Au(NP)–MWCNT-modified GCE. Linearly varying trend was the indication of diffusion-controlled electrochemical processes. In parentheses, the first term represents the slope while the second term denotes the correlation coefficient (R).
Abbreviations: Au(NPs), Au nanoparticles; GCE, glassy carbon electrode; MWCNTs, multiwalled carbon nanotubes.

zero scan rate of the plot was used to determine built-in or "formal" potential E_o, which was used to determine the corrected potential ($E_{pc}-E_o$) for all the modified electrodes. The plots of ln (I_{pc}) as a function of corrected potential ($E_{pc}-E_o$) are shown in Figure 4C, which showed a linear relation. The slope of the plot was used to determine the tendency of electron loss for bare and modified GCEs. The slope "*m*" obtained from Figure 4C and the product αn_α determined from Equation 2 were used to determine the number of electrons (*n*) participating in the oxidation or reduction of ferricyanide ions at the electrode surface as given in Equation 3:[48]

$$m = \frac{RT}{[(1-\alpha)\,n\mathrm{F}]} \tag{3}$$

The number of electrons (*n*) involved in the electrochemical reaction determined from Equation 3 was 3, 5, and 4 for bare,

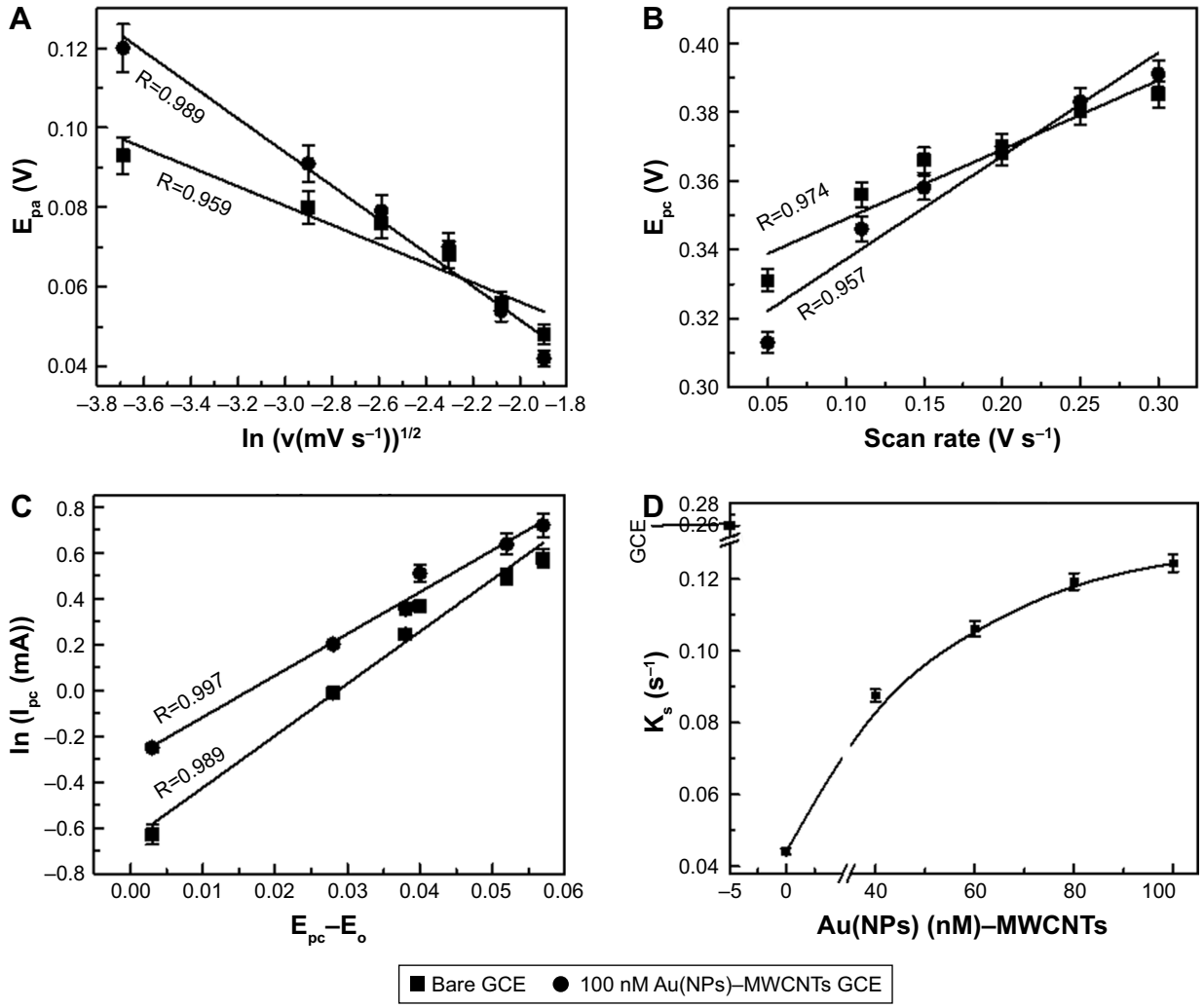

Figure 4 Plots used for the determination of number of electron transfer (n), energy transfer coefficient α, formal potential E_o and charge transfer rate constant k_s.
Notes: (**A**) Plots of E_{pa} as a function of ln ($v^{1/2}$) for bare GCE and 100 nM Au(NP)–MWCNT-modified GCE. (**B**) Plots of E_{pc} as a function of scan rate (V s^{-1}) for bare GCE and 100 nM Au(NP)–MWCNT-modified GCE. The plots were used to determine the formal potential E_o. (**C**) The plots of ln (I_{pc} (mA)) as a function of E_{pc}–E_o (V) for bare GCE and 100 nM Au(NP)–MWCNT-modified GC electrodes. The slopes of plots were used to determine the number of electrons transferred. (**D**) The rate constant k_s plotted as a function of Au(NPs) in Au(NP)–MWCNT nanohybrid-modified GCE. K_s for GCE was also added as a reference.
Abbreviations: Au(NPs), Au nanoparticles; GCE, glassy carbon electrode; MWCNTs, multiwalled carbon nanotubes.

MWCNT-, and Au(NP)–MWCNT-modified GCEs, respectively. The energy transfer coefficient α for the bare and MWCNT-modified GCE was 0.47 and 0.07, respectively, and for various concentrations of Au(NP)–MWCNT-modified GCEs, it was found in the range from 0.15 to 0.22. Ideally, α varies from 0 to 1 and classifies the type of reaction,[52] that is, irreversible if α is close to 0; reversible if it is close to 1; and quasi-reversible in case α is close to 0.5. It was observed that in the present case, the reaction was quasi-reversible for the bare GCE, became irreversible for MWCNT-modified GCE, but for Au(NP)–MWCNT nanohybrid-modified GCE, reaction again became quasi-reversible. The change in the process was affected by the different rates of charge transfer at the electrode surface for different electrodes. It was, thus, pertinent to determine the charge transfer rate constants k_s for the modified electrodes by using:[53]

$$\ln k_s = \alpha_s \ln(1-\alpha_s) + (1-\alpha_s)\ln\alpha_s - \ln\alpha_s - \ln\frac{RT}{nFv} - \alpha_s(1-\alpha_s)nF\frac{\Delta E}{RT} \quad (4)$$

where ΔE is (E_{pc}–E_{pa}) determined at different scan rates.

Thus, the dependence of rate constant k_s on the Au concentration in the nanohybrid-modified GCE as determined from Equation 4 is shown in Figure 4D, where k_s for bare GCE (=0.273±0.001 cm s^{-1}) was taken as a reference. The value of k_s was the lowest (0.044±0.001 cm s^{-1}) for MWCNT-modified GCE and then reached to a maximum of

0.124±0.001 cm s^{-1} for 100 nM Au(NP)–MWCNT-modified GCE. k_s was observed to saturate at higher concentrations of Au(NPs) in Au(NP)–MWCNT nanohybrids. The increase in Au(NPs) concentration resulted in the increase in the rate of charge transfer between the electrolytic species and modified electrode.

The choice of proper scan rate is very crucial as it leads to formation of diffusion zone near the vicinity of electrode and can affect the number of charge transferred in the reaction. Low scan rates lead to the formation of thick diffusion layer, thus reducing the flux of charge. However, fast scan rates lead to formation of thin or incomplete diffusion layer, thus resulting in high flux of charge. Also, when potential is scanned, the true potential lags the applied potential according to Equation 5.

$$E_{actual} = E_{applied}\left(1 - \frac{-t}{e^{R_\Omega C_{dl}}}\right) \quad (5)$$

where R_Ω is the ohmic resistance, C_{dl} the double-layer capacitance, and t is the time at which the measurement is taken. For slow scan rates (long *t*), the exponential approaches 0 and the errors can be negligible. In the present experiments, CV measurements were carried at a small scan rate of 0.05 V s^{-1} in 0.1 mol L^{-1} $K_4[Fe(CN)_6]$ to observe the charge transfer characteristics with varied Au(NPs) concentrations. The facilitation of charge transfer in the modified electrodes was also observed in the variation of both I_{pc} and I_{pa} with varied Au(NPs) concentrations.

The plot of redox currents (I_{pa}, I_{pc}) and ΔE (=E_{pc}–E_{pa}) as a function of Au(NPs) concentrations in Au(NP)–MWCNT nanohybrids is shown in Figure 5A and B, respectively. I_{pa}(I_{pc}) increased from –0.90 mA (0.54 mA) to –1.12 mA (0.77 mA) in the MWCNT-modified GCE with reference to the bare GCE as shown in Figure 5A. The increase in the oxidation and the reduction peak currents was due to the

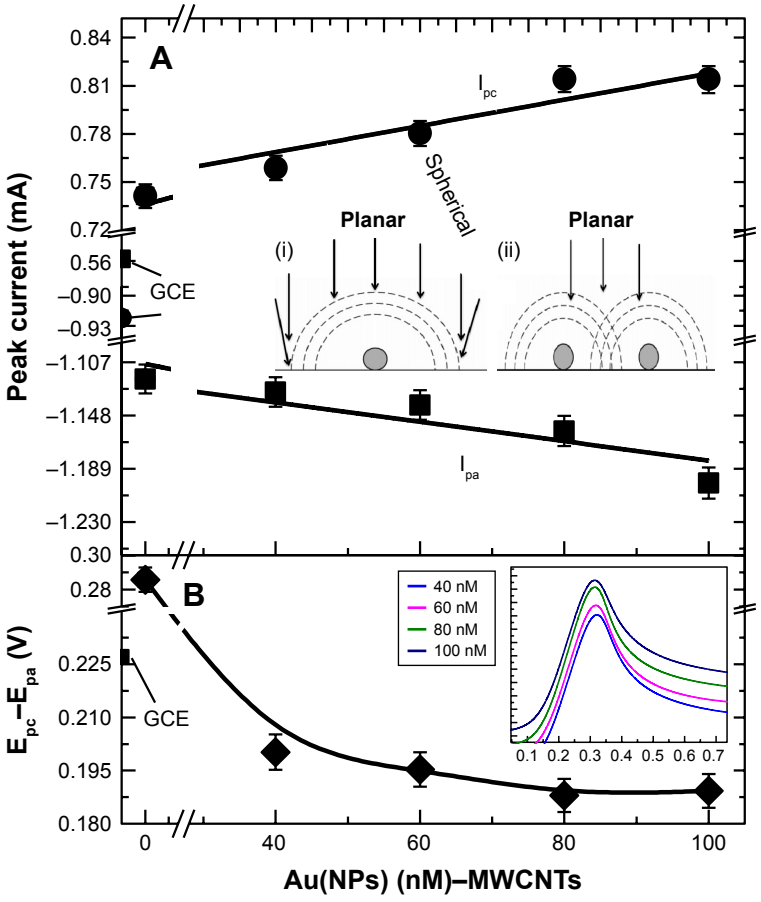

Figure 5 Plots of redox currents (I_{pa}, I_{pc}) and ΔE (=E_{pc}–E_{pa}) as a function of Au(NPs) concentrations in Au(NP)–MWCNT nanohybrids for complete understanding about symmetry of CV profile due to formation of diffusion zone around Au (NPs).

Notes: Plots of (**A**) redox peak currents I_{pc} and I_{pa}. Inset of (**A**) explains the schematic of diffusion zones around NPs. (i) Single NPs, and (ii) two NPs in very close proximity to each other. Overlapping of neighboring diffusion zones has shielded the spherical diffusion of one another. (**B**) E_{pc}–E_{pa} as a function of different Au(NPs) concentrations on MWCNT nanohybrids used for the GCE modification. Inset graph shows the CV profiles at 0.5 V s^{-1} for Au(NP)–MWCNT-modified GCE with increasing Au(NPs) concentration.

Abbreviations: Au(NPs), Au nanoparticles; GCE, glassy carbon electrode; MWCNTs, multiwalled carbon nanotubes.

presence of carboxylic groups in the MWCNT-modified GCEs. A further linear increase in I_{pa} (I_{pc}) of 5% (9%) was observed in Au(NP)–MWCNT-modified GCEs. The increase in both I_{pa} and I_{pc} was attributed to the functionalization of Au(NPs) on the surface of MWCNTs, which enhanced the electrochemical reaction for the oxidation and reduction reactions at the surface of modified electrodes. Furthermore, there was a difference in two redox potentials, that is, ΔE increased from 236±3 to 287±3 mV in the MWCNT-modified GCE with reference to bare GCE as shown in Figure 5B. However, ΔE reached its asymptotic value of 191±3 mV from 236±3 mV as the concentration of Au(NPs) was increased from 40 to 100 nM for Au(NP)–MWCNT-modified GCE.

The change in I_{pc}, I_{pa}, and ΔE ($=E_{pc}-E_{pa}$) seen with the change in Au(NPs) concentrations in the nanohybrid-modified GCEs was understood using the concept of formation of diffusion zone around Au(NPs) as explained by Dvies et al[54] and is shown in the inset of Figure 5A. Depending on the electrode surface, two diffusion zones can be formed, that is, planar diffusion zone and spherical diffusion zone, where spherical diffusion zone is efficient for the diffusion of ionic species to the electrode surface, which is due to existence of strong electric field in the zone region. Overlap of adjacent diffusion zones is expected to affect the diffusion behavior or mass transport of the ionic species to the modified electrodes. In the present case, for small concentration of Au(NPs) in Au(NP)–MWCNT nanohybrids, spherical diffusion zone (inset of Figure 5A labeled as i) was dominant over planar diffusion zone and was responsible for the electrochemical behavior. The increase in Au(NPs) concentration in the modified electrode caused the overlap of neighboring diffusion zones (inset of Figure 5A labeled as ii) and made planar diffusion dominant over spherical.[46] The effect of formation of two different zones was further observed in the CV quarter scans (positive voltage) of the nanohybrid-modified GCEs obtained at 0.5 V s^{-1} as shown in the inset of Figure 5B. For small concentrations of Au(NPs), that is, 40 and 60 nM, the symmetric CV profiles were due to spherical diffusion. However, with the increase in Au(NPs) concentration, the CV profile showed an asymmetric tail because of dominance of planar diffusion. Asymmetric behavior is just like vestigial microelectrode characteristics in which overlapping of diffusion zone has affected the shape of voltammogram.[55]

The overlap in the diffusion zones resulted in the saturation of k_s at 0.124±0.001 cm s^{-1} and asymptotic value of $E_{pc}-E_{pa}$ at 191±3 mV for higher concentrations of Au(NPs) in the nanohybrid-modified electrode. This possibly showed that there was a limit of the Au(NPs) concentration in the nanohybrid to achieve optimal performance. The charge transfer characteristics were further probed by the EIS.

EIS analysis of Au(NP)–MWCNT-modified GCE

EIS was also performed for the bare, MWCNT-, and Au(NP)–MWCNT-modified GCEs and the corresponding Nyquist plots are shown in Figure 6A. A linear relation between Z' and –Z" for GCE (bottom Nyquist plot) was observed with a slope of 0.97±0.01, which also confirmed that the reaction kinematics were diffusion-limited processes.[56]

The Nyquist plot was used to draw the equivalent Randle's circuit and is shown in the inset of Figure 6A. The equivalent circuit contained uncompensated solution resistance R_s, double-layer capacitance C_{ad}, which was related to delamination of coating, mass-transport contribution Z_w, that is, ion diffusion, and the constant phase element, CPE. The values of each element, R_s, C_{ad}, and Z_w obtained from the fitting of Nyquist plots for each modified electrode are given in Table 1. The variation in Warburg resistance Z_w is shown in Figure 6B as a function of Au(NPs) concentration in the nanohybrid-modified GCEs. The first point in the plot is for the bare electrode shown for reference. Z_w first dropped from 6.32±0.05 mS for bare GCE to 1.10±0.05 mS for MWCNT-modified GCE. It then increased to 5.67±0.05 mS for 80 nM Au(NPs) in the nanohybrid-modified electrode. The drop in Z_w for the MWCNT-modified electrode suggested reduced ionic diffusion to reach the electrode surface. The increase in the Z_w for Au(NP)–MWCNT nanohybrids suggested efficient ionic diffusion, which resulted in increased charge transfer. The solution resistance R_s, which is the resistance offered by electrolytic solution, is plotted as a function of Au(NPs) and is shown in Figure 6C. R_s increased to a maximum of 82.5 Ω for MWCNT-modified GCE. However, R_s dropped to 50.0±0.5 Ω for 80 nM Au(NPs) nanohybrid-modified GCE. An increase in Z_w to 5.67±0.05 mS and decrease in R_s to 50.0±0.5 Ω with the increase in the concentration of Au(NPs) was due to enhanced charge transfer characteristics for Au(NP)–MWCNT-modified GCE.

From the above discussion, it can be deduced that the charge transfer characteristics can be controlled by varying the concentration of Au(NPs) in Au(NP)–MWCNT nanohybrid to a certain limit. The CV and EIS studies confirmed the diffusion-controlled processes in the charge transfer between the modified electrode and electrolytic solution. The diffusion processes were quasi-reversible (α=0.22) in Au(NP)–MWCNT nanohybrid-modified electrodes with a charge transfer rate k_s of 0.124±0.001 cm s^{-1}. An increase in

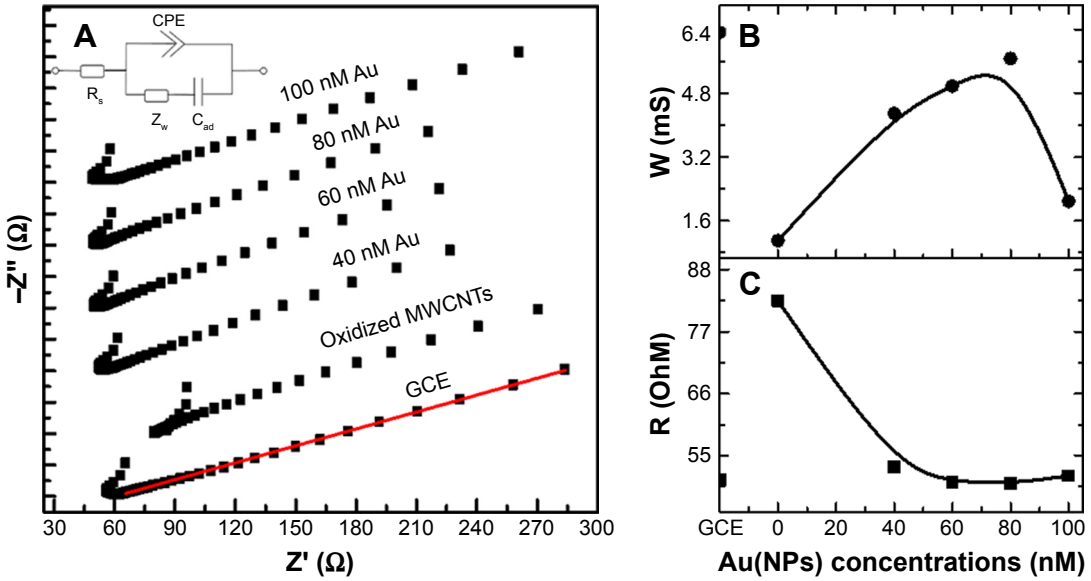

Figure 6 Electrochemical impedance spectroscopy of GCE, MWCNTs-modified GCE and Au(NP)-MWCNTs -modified GCE.
Notes: (**A**) Nyquist plots between Z' and –Z'' for GCE, MWCNT-modified GCE, 40 nM Au(NP)–MWCNT-modified GCE, 60 nM Au(NP)–MWCNT-modified GCE, 80 nM Au(NP)–MWCNT-modified GCE, and 100 nM Au(NP)–MWCNT-modified GCE in 0.1 mol L^{-1} $K_4[Fe(CN)_6]$. Red line in the bottom Nyquist plot represents the fitted data used to calculate the slope of linear region. Inset is the Randle circuit used for the fitting of Nyquist plots. R_s represents the solution resistance, CPE is the constant-phase element, Z_W is the Warburg coefficient, C_{ad} is the double-layer capacitance. (**B**, **C**) Plot of W and R_s as a function of Au(NPs) concentration on the surface of MWCNT nanohybrid-modified GCE.
Abbreviations: Au(NPs), Au nanoparticles; GCE, glassy carbon electrode; MWCNTs, multiwalled carbon nanotubes.

the value of k_s with the increase in concentration of Au(NPs) in nanohybrid-modified electrodes was due to enhanced charge transfer rate, which led to increase in $I_{pc}(I_{pa})$. The characteristics of charge transfer in the modified electrodes were further studied with the attachment of different concentrations of *E. coli*.

Electrochemical response of modified electrodes against *E. coli*

The electrochemical behavior of the modified electrodes was determined for different concentrations of *E. coli* (10^4, 10^5, and 10^6/mL in 0.1 mol L^{-1} $K_4[Fe(CN)_6]$). Figure 7A and B shows the CV scans at the rate of 0.05 V s^{-1} for various concentrations of *E. coli* attached to Figure 7A 40 nM and Figure 7B 80 nM Au(NPs) in nanohybrid-modified GCEs. The CV profiles are displaced vertically for clarity and the horizontal line in each graph is at y=0. The dotted vertical lines were drawn to demonstrate the change in the position of E_{pc} and E_{pa}. The bottom three rows in each part of Figure 7A and B are the CV profiles for the bare, MWCNTs, and Au(NPs)–MWCNTs in the nanohybrid-modified GCEs. The top three scans in each part of Figure 7A and B show the CV profiles of the nanohybrid-modified GCEs exposed to various concentrations of *E. coli* in the range from 10^4 to 10^6/mL. It is shown in Figure 7A and B that the attachment of *E. coli* resulted in increase of redox current in nanohybrid-modified electrodes because of transfer of electrons through two glutathione enzymes from *E. coli*.[57]

Table 1 Value of different variables such as R_s, CPE, C_{ad}, and Z_w used for the fitting of Nyquist plots of GCE, MWCNT GCE, and Au(NP)–MWCNT GCE

Electrodes modified	R_s (Ω) (±0.5)	CPE (mMho)/N (±0.05)	C_{ad} (mF) (±0.05)	Z_w (mMho) (±0.05)
GCE	50.7	3.27/0.405	2.25	1.61
MWCNT GCE	82.5	4.49/0.493	0.38	1.10
40 nM Au(NP)–MWCNT GCE	53.0	3.42/0.399	2.85	4.29
60 nM Au(NP)–MWCNT GCE	50.3	3.72/0.41	2.21	4.98
80 nM Au(NP)–MWCNT GCE	50.0	3.85/0.387	2.60	5.67
100 nM Au(NP)–MWCNT GCE	51.4	3.21/0.403	2.69	2.09

Abbreviations: Au(NP), Au nanoparticle; GCE, glassy carbon electrode; MWCNTs, multiwalled carbon nanotubes.

The increase in both I_{pa} and I_{pc} as a function of *E. coli* was used to estimate the dependence of sensitivity of the nanohybrid-modified GCEs on Au(NPs) concentration to detect *E. coli* as shown in Figure 8A–D. In Figure 8, the first two points on x-axis in each plot are for bare and MWCNT-modified GCEs as reference, respectively. The increase in $I_{pc}(I_{pa})$ observed was 2% (2%), 9% (3%), 13% (7%), and 2% (5%) for 40, 60, 80, and 100 nM Au(NPs) concentrations in nanohybrid-modified electrodes, respectively. The difference in the rate of increase of both I_{pc} and I_{pa} peak

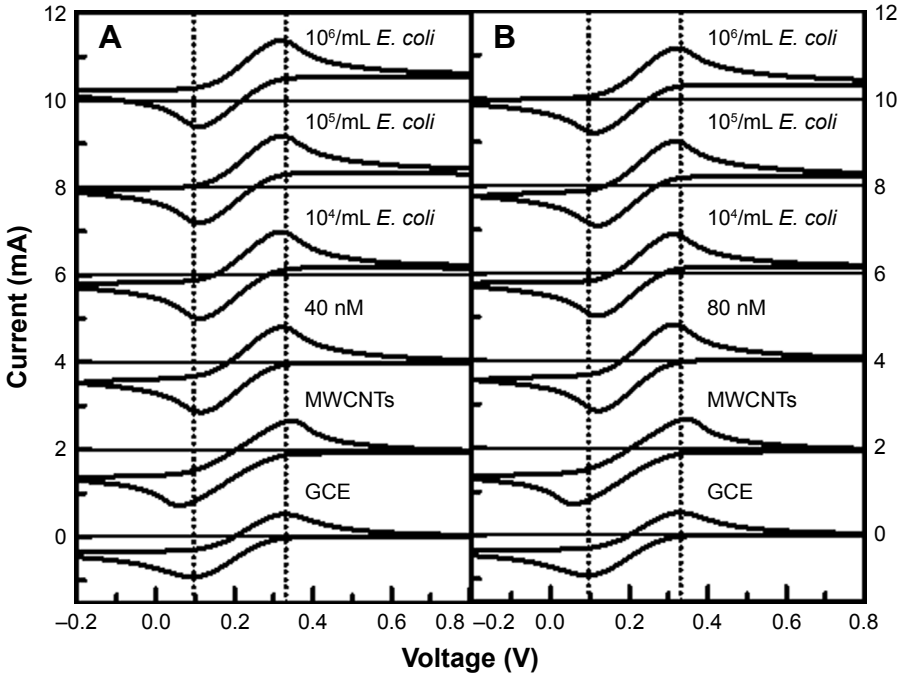

Figure 7 CV plots of the Au(NP)–MWCNT-modified GCE in 0.1 mol L^{-1} $K_4[Fe(CN)_6]$ at 0.05 V s^{-1} for different concentrations of *Escherichia coli* 10^4, 10^5, and 10^6/mL.
Note: (**A**) 40 nM Au(NP)–MWCNT-modified GCE, and (**B**) 80 nM Au(NP)–MWCNT-modified GCE.
Abbreviations: Au(NPs), Au nanoparticles; GCE, glassy carbon electrode; CV, cyclic voltammetery; MWCNTs, multiwalled carbon nanotubes.

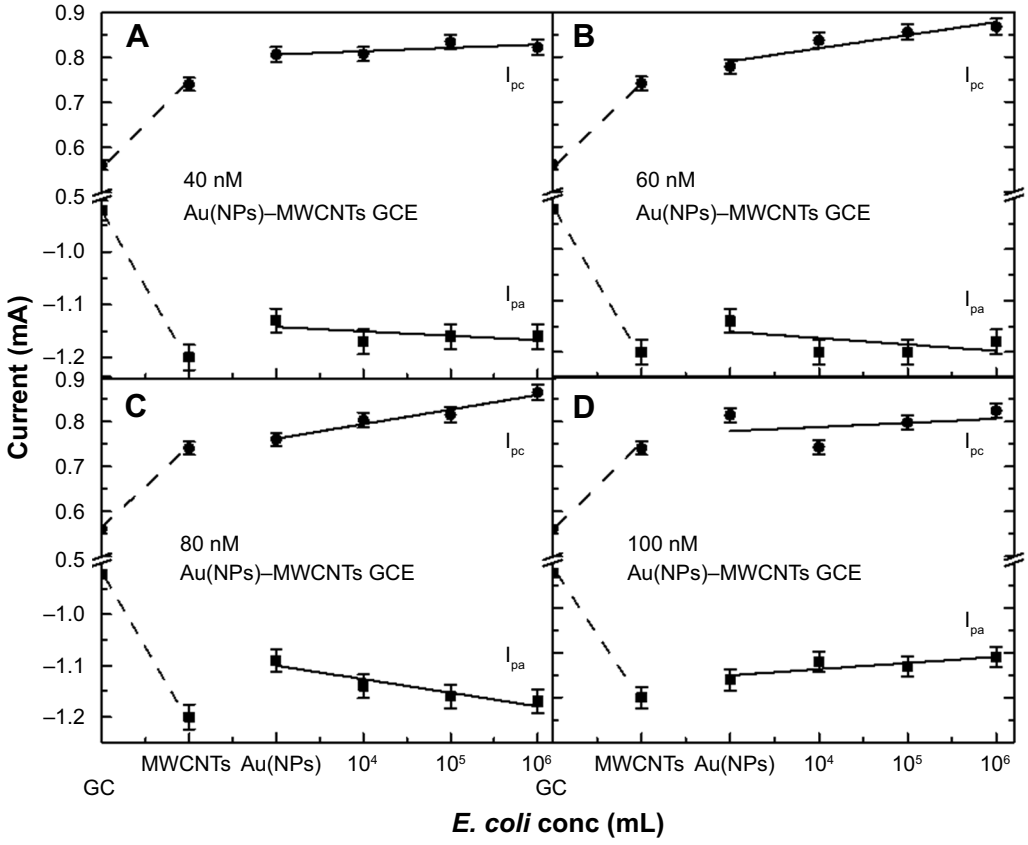

Figure 8 Plots of I_{pc} and I_{pa} as a function of different *Escherichia coli* concentrations on Au(NP)–MWCNT-modified GCE.
Notes: I_{pc} and I_{pa} for GCE and MWCNT-modified GCE were also shown for the reference (first two points on x-axis in each graph). (**A**) 40 nM Au(NP)–MWCNT-modified GCE, (**B**) 60 nM Au(NP)–MWCNT-modified GCE, (**C**) 80 nM Au(NP)–MWCNT-modified GCE, and (**D**) 100 nM Au(NP)–MWCNT-modified GCE. I_{pc} has changed linearly for 40, 60, and 80 nM Au(NP)–MWCNT nanohybrids with increased concentration of *E. coli*.
Abbreviations: Au(NPs), Au nanoparticles; GCE, glassy carbon electrode; MWCNTs, multiwalled carbon nanotubes.

current values with *E. coli* concentrations demonstrated that the conductivity and electrochemical catalytic properties of nanohybrid had a synergistic effect on the detection of *E. coli*. This could be attributed to the varied concentrations of Au(NPs) on the surface of the MWCNTs. In case of low concentrations of Au(NPs) such as 40 and 60 nM, the charge transfer rate was low, that is, k_s=0.08 s^{-1}, which delayed the charge transfer between *E. coli* and nanohybrid-modified electrodes. For 80 nM Au(NP)–MWCNT-modified GCE, high value of k_s was 0.11 s^{-1}, which resulted in efficient charge transfer between Au(NP)–MWCNT-modified GCE and ferrocyanide ions in the presence of *E. coli*. For 100 nM concentration of Au(NPs), the observed drop in the redox current was attributed to the dominance of planar diffusion, which reduced the diffusion of ions. This behavior revealed that a suitable concentration of Au(NPs) had an important role for the charge transfer characteristics between the modified electrode and electrolytic solution. On the basis of these results, it is concluded that Au(NPs) functionalized on MWCNTs facilitate enhanced charge transfer with increasing concentrations of Au(NPs).

The limit of detection (LoD) and limit of quantitation (LoQ) values were also determined for each Au concentration of modified GCE in *E. coli* surroundings by using Equation 6:

$$LOD = \frac{3\sigma}{M} \text{ and } LOQ = \frac{10\sigma}{M} \quad (6)$$

where σ is the standard deviation of the peak currents and M is the slope of the working curve. LoD for 40, 60, 80, and 100 nM Au(NP)–MWCNT nanohybrids were 5.57±0.03×10^3/mL, 4.38±0.03×10^3/mL, 4.03±0.03×10^3/mL, and 1.20±0.03×10^4/mL, respectively, while LoQ for 40, 60, 80, and 100 nM Au(NP)–MWCNT nanohybrids were 1.85±0.03×10^3/mL, 1.46±0.03×10^3/mL, 1.34±0.03×10^3/mL, and 4.00±0.03×10^4/mL, respectively. The lowest values of LoD and LoQ have been shown by 80 nM Au(NP)–MWCNT nanohybrids. Decreased value of LoD and LoQ with increased Au(NPs) concentration functionalized on MWCNTs has shown the enhanced charge transfer. The findings of the present work were compared with the already existing results and are summarized in Table 2. It is significant to note that the sensor suggested in the present work has relatively low LoD and overall performance lies well within the range of those reported in the literature. The reproducibility of the sensor was determined by repeating the measurements with each concentration (40–100 nM) of Au(NPs) under the same condition for three different electrodes. An relative standard deviation value of 5% was obtained in the measured oxidation current, which indicated the good reproducibility of reported sensor. This showed that the fabricated device was reliable and reproducible.

Table 2 Comparison of results obtained in the present work with the literature for the LoD

Detection technique	Sensing element	LoD (*Escherichia coli*)
Paper-based ELISA method[58]	Filter paper was pretreated with chitosan and glutaraldehyde	1×10^4 CFU/mL
Immunoassay[59]	Lateral flow immunoassay	10^5 CFU/mL
Immunofluorescence[60]	Immunofluorescence strip sensor	10^5 CFU/mL
Immunosensing[61]	Electrocatalytic gold nanoparticle tags	3.09×10^2 CFU/mL
AIEE[62]	AIE-based fluorescent self-assembled glycoacrylamides	7.30×10^5 cells/mL
Present work	Au(NP)/MWCNT-modified GCE	1.34×10^3 cells/mL

Abbreviations: AIEE, aggregation-induced emission enhancement; Au(NPs), Au nanoparticles; CFU, colony-forming unit; ELISA, enzyme-linked immunosorbent assay; GCE, glassy carbon electrode; LoD, limit of detection; MWCNTs, multiwalled carbon nanotubes.

Conclusion

The present study demonstrated the critical role of concentration of Au(NPs) in the electrochemical response of Au(NP)–MWCNT-modified electrodes. The increase in the number of electrons in the electrochemical reaction was significant in the Au(NP)–MWCNT nanohybrids as compared to bare GCE. The rate of charge transfer was also dependent on the concentration of Au(NPs), which increased from 0.044±0.001 cm s^{-1} for MWCNT-modified GCE to 0.124±0.001 cm s^{-1} for 80 nM Au(NP)–MWCNT-modified GCE. This was due to enhanced redox reaction in the presence of nanohybrid electrodes. EIS measurements also confirmed that increase in mass transfer by 5 times was the highest when 80 nM concentration of Au(NPs) was present in the nanohybrid-modified electrodes. Electrochemical behavior of Au(NP)-modified electrodes to the *E. coli* was also maximum for 80 nM concentration of Au(NPs) in the nanohybrid-modified electrode and a maximum increase of 13% in I_{pc} was observed. The increased number of charge transfer and enhanced rate of charge transfer were attributed to the formation of spherical diffusion zones around the modified electrodes, which showed strong dependence on the concentration of Au(NPs) in the nanohybrids. High concentration of Au(NPs) in nanohybrids led to formation of planar diffusion zones, which led to reduced number of charge transfer and transfer rates.

Acknowledgments

Research work was funded by HEC NRPU grant 261 and 1770. SM is thankful to Higher Education Commission for a PhD scholarship. Authors are thankful to Dr H Ismail and Prof Dr B Mirza from Department of Biochemistry, Faculty of Biological Sciences, Quaid-i-Azam University, Islamabad, Pakistan, for providing *Escherichia coli* and also to Dr Sana from Department of Physics, COMSATS Institute of Information Technology, Islamabad, Pakistan, for synthesis of Au(NPs).

Disclosure

The authors report no conflicts of interest in this work.

References

1. Şahin B, Demir E, Aygun A, et al. Investigation of the effect of pomegranate extract and monodisperse silver nanoparticle combination on MCF-7 cell line. *J Biotechnol*. 2017;260(1):79–83.
2. Oliveira MD, Correia MT, Diniz FB. Concanavalin A and polyvinyl butyral use as a potential dengue electrochemical biosensor. *Biosens Bioelectron*. 2009;25(4):728–732.
3. Iverson NM, Barone PW, Shandell M, et al. In vivo biosensing via tissue-localizable near-infrared-fluorescent single-walled carbon nanotubes. *Nat Nanotechnol*. 2013;8(11):873–880.
4. Kim JH, Patra CR, Arkalgud JR, et al. Single-molecule detection of H_2O_2 mediating angiogenic redox signaling on fluorescent single-walled carbon nanotube array. *ACS Nano*. 2011;5(10):7848–7857.
5. Parveen S, Misra R, Sahoo SK. Nanoparticles: a boon to drug delivery, therapeutics, diagnostics and imaging. *Nanomed Nanotechnol*. 2012;8(2):147–166.
6. Zhang J, Landry MP, Barone PW, et al. Molecular recognition using corona phase complexes made of synthetic polymers adsorbed on carbon nanotubes. *Nat Nanotechnol*. 2013;8(12):959–968.
7. Bozkurt S, Tosun B, Sen B, et al. A hydrogen peroxide sensor based on TNM functionalized reduced graphene oxide grafted with highly monodisperse Pd nanoparticles. *Anal Chim Acta*. 2017;989(1):88–94.
8. Boghossian AA, Sen F, Gibbons BM, et al. Application of nanoparticle antioxidants to enable hyperstable chloroplasts for solar energy harvesting. *Adva Energy Mat*. 2013;3(7):881–893.
9. Giraldo JP, Landry MP, Faltermeier SM, et al. Plant nanobionics approach to augment photosynthesis and biochemical sensing. *Nat Mater*. 2014;13(4):400–408.
10. Chen SW, Murray RW. Electrochemical quantized capacitance charging of surface ensembles of gold nanoparticles. *J Phys Chem B*. 1999;103(45):9996–10000.
11. Li J, Yamada Y, Murakoshi K, Nakato Y. Sustainable metal nanocontacts showing quantized conductance prepared at a gap of thin metal wires in solution. *Chem Commun*. 2001;1(21):2170–2171.
12. Haruta M. Size- and support-dependency in the catalysis of gold. *Catal Today*. 1997;36(1):153–166.
13. Subramanian V, Wolf EE, Kamat PV. Green emission to probe photoinduced charging events in ZnO-Au nanoparticles. Charge distribution and fermi-level equilibration. *J Phys Chem B*. 2003;107(1):7479–7485.
14. Iijima S. Helical microtubules of graphitic carbon. *Nature*. 1991;354(6348):56–58.
15. Wang YR, Ping H, Liang QL, Guo L, Wang YM. Application of carbon nanotube modified electrode in bioelectroanalysis. *China J Anal Chem*. 2008;36(8):1011–1016.
16. Gao C, Li W, Jin YZ, Kong H. Facile and large-scale synthesis and characterization of carbon nanotube/silver nanocrystal nanohybrids. *Nanotechnology*. 2006;17(12):2882–2890.
17. Liu XS, Hu F, Zhu DR, et al. One-step synthesis of carbon nanotubes with Ni nanoparticles as a catalyst by the microwave-assisted polyol method. *J Alloy Compd*. 2011;509(6):2829–2832.
18. Sowichai K, Supothina S, Nimittrakoolchai OU, Seto T, Otani Y, Charinpanitkul T. Facile method to prepare magnetic multi-walled carbon nanotubes by in situ co-precipitation route. *J Ind Eng Chem*. 2012;18(5):1568–1571.
19. Zheng R, XianSong L, Feng H, et al. One-step preparation of carbon nanotubes with nickel as the core. *Sci China Technol Sci*. 2011;54(1):76–80.
20. Eder D. Carbon nanotube–inorganic hybrids. *Chem Rev*. 2010;110(3):1348–1385.
21. Jeong HY, Kim JY, Kim JW, et al. Graphene oxide thin films for flexible nonvolatile memory applications. *Nano Lett*. 2010;10(11):4381–4386.
22. Yadav SK, Madeshwaran SR, Cho JW. Synthesis of a hybrid assembly composed of titanium dioxide nanoparticles and thin multi-walled carbon nanotubes using "click chemistry." *J Colloid Interface Sci*. 2011;358(2):471–476.
23. Gupta V, Kotnala RK. Multifunctional ferromagnetic carbon-nanotube arrays prepared by pulse-injection chemical vapor deposition. *Angew Chem Int Ed Engl*. 2012;51(12):2916–2919.
24. Hrapovic S, Liu Y, Male KB et al. Electrochemical biosensing platforms using platinum nanoparticles and carbon nanotubes. *Anal Chem*. 2004;76(4):1083–1088.
25. Wu HY, Hu SS. The fabrication of a colloidal gold–carbon nanotubes composite film on a gold electrode and its application for the determination of cytochrome c. *Colloid Surf B Biointerfaces*. 2005;41(4):299–304.
26. Huang XJ, Li CC, Gu B, Kim JH, Cho SO, Choi YK. Controlled molecularly mediated assembly of gold nanooctahedra for a glucose biosensor. *J Phys Chem C*. 2008;112(10):3605–3611.
27. Bui MPN, Pham XH, Han KN, et al. Electrochemical sensing of hydroxylamine by gold nanoparticles on single-walled carbon nanotube films. *Electrochem Commun*. 2010;12(2):250–253.
28. Jha N, Ramaprabhu S. Development of Au nanoparticles dispersed carbon nanotube-based biosensor for the detection of paraoxon. *Nanoscale*. 2010;2(5):806–810.
29. Favero G, Fusco G, Mazzei F, Tasca F, Antiochia R. Electrochemical characterization of graphene and MWCNTs screen-printed electrodes modified with aunps for laccase biosensor development. *Nanomaterials (Basel)*. 2015;5(4):1995–2006.
30. Zhang X, Huang C, Jiang Y, et al. An electrochemical glycan biosensor based on a thionine-bridged multiwalled carbon nanotube/gold nanoparticle composite-modified electrode. *RSC Adv*. 2016;6(114):112981–112987.
31. Li C, Su Y, Lv X, Xia H, Wang Y. Electrochemical acetylene sensor based on Au/MWCNTs. *Sensor Actuat B Chem*. 2010;149(2):427–431.
32. Dong J, Zhao H, Xu M, Ma Q, Ai S. A label-free electrochemical impedance immunosensor based on AuNPs/PAMAM-MWCNT-Chi nanocomposite modified glassy carbon electrode for detection of Salmonella typhimurium in milk. *Food Chem*. 2013;141(3):1980–1986.
33. Bai J, Zhang X, Peng Y, et al. Ultrasensitive sensing of diethylstilbestrol based on AuNPs/MWCNTs-CS composites coupling with sol-gel molecularly imprinted polymer as a recognition element of an electrochemical sensor. *Sens Actuat B Chem*. 2017;238(1):420–426.
34. Kan X, Zhang T, Zhong M, Lu X. CD/AuNPs/MWCNTs based electrochemical sensor for quercetin dual-signal detection. *Biosens Bioelectron*. 2016;77(1):638–643.
35. Hao YU, Xiao FENG, Xiao-Xia CHEN, et al. Electrochemical determination of bisphenol a on a glassy carbon electrode modified with gold nanoparticles loaded on reduced graphene oxide-multi walled carbon nanotubes composite. *Chinese J Anal Chem*. 2017;45(5):713–720.
36. Gorby YA, Yanina S, McLean JS, et al. Electrically conductive bacterial nanowires produced by Shewanella oneidensis strain MR-1 and other microorganisms. *Proc Natl Acad Sci U S A*. 2006;103(30):11358–11363.

37. Zhang T, Cui CZ, Chen S, Yang H, Shen P. The direct electrocatalysis of *Escherichia coli* through electroactivated excretion in microbial fuel cell. *Electrochem Commun*. 2008;10(2):293–297.
38. Park DH, Zeikus JG. Improved fuel cell and electrode designs for producing electricity from microbial degradation. *Biotechnol Bioeng*. 2003;81(3):348–355.
39. Ringeisen BR, Henderson E, Wu PK, et al. High power density from a miniature microbial fuel cell using Shewanella oneidensis DSP10. *Environ Sci Technol*. 2006;40(8):2629–2634.
40. Yia H, Nevin KP, Kim BC, et al. Selection of a variant of Geobacter sulfurreducens with enhanced capacity for current production in microbial fuel cells. *Biosens Bioelectron*. 2009;24(12):3498–3503.
41. Gu L, Luo PG, Wang H, et al. Single-walled carbon nanotube as a unique scaffold for the multivalent display of sugars. *Biomacromolecules*. 2008; 9(9):2408–2418.
42. Li R, Wu K, Liu C, et al. 4-Amino-1-(3-mercapto-propyl)-pyridine hexafluorophosphate ionic liquid functionalized gold nanoparticles for IgG immunosensing enhancement. *Anal Chem*. 2014;86(11):5300–5307.
43. Liu H, Xu S, He Z, et al. Supersandwich cytosensor for selective and ultrasensitive detection of cancer cells using aptamer-DNA concatamer-quantum dots probes. *Anal Chem*. 2013;85(6):3385–3392.
44. Dilonardo E, Penza M, Alvisi M, et al. Electrophoretic deposition of Au NPs on MWCNT-based gas sensor for tailored gas detection with enhanced sensing properties. *Sens Actuat B Chem*. 2016;223(1): 417–428.
45. Dilonardo E, Penza M, Alvisi M, et al. Electrophoretic deposition of Au NPs on CNT networks for sensitive NO_2 detection. *J Sens Sens Syst*. 2014;3(2):245–252.
46. Mehmood S, Naeem A, Sabahat S, et al. Modified structural and optical characteristics of Au-NPs–MWCNTs nanohybrids. *Superlattice Microst*. 2015;81(1):248–264.
47. Hajian R, Yusof NA, Faragi T, Shams N. Fabrication of an electrochemical sensor based on gold nanoparticles/carbon nanotubes as nanocomposite materials: determination of myricetin in some drinks. *PLoS One*. 2014;9(5):1–7.
48. Yue D, Jia Y, Yao Y, Sun J, Jing Y. Structure and electrochemical behavior of ionic liquid analogue based on choline chloride and urea. *Electrochim Acta*. 2012;65(1):30–36.
49. Zhao YD, Bi YH, Zhang WD, Luo QM. The interface behavior of hemoglobin at carbon nanotube and the detection for H_2O_2. *Talanta*. 2005;65(2):489–494.
50. Zhao GC, Yin ZZ, Zhang L, Wei XW. Direct electrochemistry of cytochrome c on a multi-walled carbon nanotubes modified electrode and its electrocatalytic activity for the reduction of H_2O_2. *Electrochem Commun*. 2005;7(3):1887–1890.
51. Liu X, Shi L, Niu W, Li H, Xu G. Amperometric glucose biosensor based on single-walled carbon nanohorns. *Biosens Bioelectron*. 2008; 23(12):1887–1890.
52. Rafiee B, Fakhari AR, Ghaffarzadeh M. Impedimetric and stripping voltammetric determination of methamphetamine at gold nanoparticles-multiwalled carbon nanotubes modified screen printed electrode. *Sensor Actuat B*. 2015;218(1):271–279.
53. Laviron E. General expression of the linear potential sweep voltammogram in the case of diffusionless electrochemical systems. *J Electroanal Chem*. 1979;101(1):19–28.
54. Dvies TJ, Banks CE, Compton RG. Voltammetry at spatially heterogeneous electrodes. *J Solid State Electr*. 2005;9(12):797–808.
55. Davies TJ, Compton RG. The cyclic and linear sweep voltammetry of regular and random arrays of microdisc electrodes: theory. *J Electroanal Chem*. 2005;585(1):63–82.
56. Suni II. Impedance methods for electrochemical sensors using nanomaterials. *TrAC Trend Anal Chem*. 2008;27(7):604–611.
57. Chalenko Y, Shumyantsev V, Ermolaev S, Archakov A. Electrochemistry of *Escherichia coli* JM109: direct electron transfer and antibiotic resistance. *Biosens Bioelectron*. 2012;32(1):219–233.
58. Pang B, Zhao C, Li L, et al. Development of a low-cost paper-based ELISA method for rapid *Escherichia coli* O157: H7 detection. *Anal Biochem*. 2018;542(1):58–62.
59. Song C, Liu J, Li J, Liu Q. Dual FITC lateralflow immunoassay for sensitive detection of *Escherichia coli* O157: H7 in food samples. *Biosens Bioelctron*. 2016;85(1):734–739.
60. Song C, Li J, Liu J, et al. Simple sensitive rapid detection of *Escherichia coli* O157: H7 in food samples by label-free immunofluorescence strip sensor. *Talanta*. 2016;156(1):42–47.
61. Hassan ARHAA, Muniz ADLE, Merkoçi A. Highly sensitive and rapid determination of *Escherichia coli* O157: H7 in minced beef and water using electrocatalytic gold nanoparticle tags. *Biosens Bioelectron*. 2015;67(1):511–515.
62. Ajish JK, Kumar KA, Ruhela A, Subramanian M, Ballal AD, Kumar M. AIE based fluorescent self assembled glycoacrylamides for *E. coli* detection and cell imaging. *Sens Actuat B Chem*. 2018;255(1):1726–1734.